

# Unidirectional Photonic Reflector Using a Defective Atomic Lattice

Tianming Li,<sup>1,2</sup> Hong Yang,<sup>1,\*</sup> Maohua Wang,<sup>3</sup> Chengping Yin,<sup>2</sup> Tinggui Zhang,<sup>4,†</sup> and Yan Zhang<sup>3,‡</sup>

<sup>1</sup>*School of Physics and Electronic Engineering, Hainan Normal University, Haikou 571158, P. R. China*

<sup>2</sup>*School of Physics and Telecommunication Engineering,  
South China Normal University, Guangzhou 510006, P. R. China*

<sup>3</sup>*Center for Quantum Sciences and School of Physics,  
Northeast Normal University, Changchun 130024, P. R. China*

<sup>4</sup>*School of Mathematics and Statistics, Hainan Normal University, Haikou 571158, P. R. China*

(Dated: October 16, 2023)

Based on the broken spatial symmetry, we propose a novel scheme for engineering a unidirectional photonic reflector using a one-dimensional atomic lattice with defective cells that have been specifically designed to be vacant. By trapping three-level atoms and driving them into the regime of electromagnetically induced transparency, and through the skillful design of the number and position of vacant cells in the lattice, numerical simulations demonstrate that a broad and high unidirectional reflection region can be realized within EIT window. This proposed unidirectional reflector scheme provides a new platform for achieving optical nonreciprocity and has potential applications for designing optical circuits and devices of nonreciprocity at extremely low energy levels.

In order to achieve the practical applications of nonreciprocal photonic devices and circuits without the use of magneto-optical materials, which can hinder miniaturization and integration, such as chip isolators, circulators, and all-optical diodes [1–6], the research on controllable unidirectional light propagation to induce a symmetry-breaking effect is of great significance within the science and engineering disciplines [7–10]. Various strategies for achieving optical nonreciprocity have been explored, such as breaking the time-reversal symmetry [11] in atom-cavity systems [12], optomechanical systems [13–16], magnomechanical systems [17, 18], giant-atom systems [11], quantum squeezing resonator modes in chip systems [19], and considering Doppler shifts in hot atomic systems [20–22].

In recent years, significant progress has been made in the study of unidirectional reflection (Here, the unidirectional reflection, i.e., the perfectly asymmetric reflection, indicates that the reflection of the wave incident from one side is completely suppressed when the wave incident from the other side is typically reflected.) of nonlinear materials in various physical systems. For instance, by trapping atoms in space with a moving optical lattice, a probe pulse propagating along the lattice from two sides could experience nonreciprocal reflection [23–25]; however, the implementation of moving lattices requires relatively high technological requirements. For a static optical lattice, by skillfully coupling it with standing-wave fields for a dynamic frequency shift as a cosine/sine function of the lattice position, the initially uniform probe susceptibility can be modulated to satisfy optical parity-time (PT) symmetry (antisymmetric) [26–28], leading to unidirectional reflectionless. In addition, unidirectional reflection can be achieved in continuous media when the

refractive index obeys the spatial Kramers-Kronig (KK) relations [29–31]. However, the main difficulty in implementing these schemes lies in the need for precise modulation, including achieving a balance of gain and loss within a single period, precisely arranging the spatial coupling fields, skillfully constructing spatial-KK media, and improving the low reflectivity of unidirectional reflection.

As one of the approaches to achieving a photonic bandgap (PBG) [32, 33], the use of an atomic lattice has been employed to attain a large Bragg reflection [34–36]. In particular, by driving periodically trapped atoms into the regime of electromagnetically induced transparency (EIT), we can significantly enhance the reflectivity and achieve additional PBGs and greater tunability [37, 38]. Furthermore, such reciprocal reflection is robust against disorder in the atomic lattice while maintaining periodicity [39], but can be disrupted in a defective atomic lattice as we found [40]. Maybe, distinct and intriguing reflection phenomena will be observed, in a purposely designed defective lattice.

In this study, we propose a novel scheme to achieve unidirectional reflection using a one-dimensional (1D) defective atomic lattice, comprising both filled lattice cells (trapping atoms) and vacant cells (not trapping atoms). Firstly, we drive the atoms into a three-level  $\Lambda$ -type EIT system [see Fig.1(a)]. Subsequently, we engineer the lattice into two parts of periodic structures: Part I with  $p_1$  periods, each consisting of  $a_f$  filled cells and  $a_v$  vacant cells, and Part II with  $p_2$  periods of solely filled cells [see Fig.1(b)]. The total length of the lattice is  $L = S\lambda_0$ , where  $S = (a_f + a_v)p_1 + p_2$ . Our proposal utilizes vacant cells to break spatial symmetry, inducing unidirectional reflection with high reflectivity in the EIT window.

We consider cold  $^{87}\text{Rb}$  atoms that are trapped and driven by two coherent fields, as depicted in Fig. 1(a). The weak probe field with frequency  $\omega_p$  (amplitude  $\mathbf{E}_p$ ), and the strong coupling field with frequency  $\omega_c$  (amplitude  $\mathbf{E}_c$ ). The fields  $\omega_p$  and  $\omega_c$  interact via the dipole-allowed transitions  $|1\rangle \leftrightarrow |3\rangle$  and  $|2\rangle \leftrightarrow |3\rangle$ , respec-

\* yang'hongbj@126.com

† tinggui333@163.com

‡ zhangy345@nenu.edu.cn

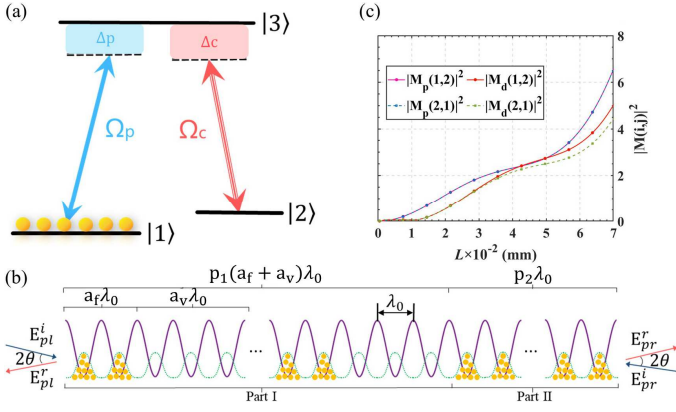


FIG. 1. (color online) (a) Energy level diagram of a three-level  $\Lambda$ -type atomic system interacting with a weak probe field  $\Omega_p$  and a strong coupling field  $\Omega_c$ . (b) 1D defective atomic lattice with the width  $\lambda_0$  for each period, which comprises Part I and Part II. The probe field  $\mathbf{E}_p$  is incident from either the left side (denoted by  $\mathbf{E}_{pl}^i$ ) or the right side (denoted by  $\mathbf{E}_{pr}^i$ ) with a small incident angle  $\theta$  relative to  $x$ -axis. The relevant reflected fields are denoted by  $\mathbf{E}_{pl}^r$  and  $\mathbf{E}_{pr}^r$ . (c) The Square of moduli of matrix elements  $M_{p,d}(1,2)$ ,  $M_{p,d}(2,1)$  as functions of length  $L$ , for a perfect lattice with 180 fulfilled cells and a defective lattice with  $a_f = 5$ ,  $a_v = 25$ ,  $p_1 = 1$ ,  $p_2 = 150$ , respectively. The parameters are  $\Gamma_{31} = \Gamma_{21} = 6.0$  MHz,  $\Omega_c = 36.0$  MHz,  $\Delta_c = 15.0$  MHz,  $\lambda_{Lat} = 781.3$  nm,  $\lambda_{31} = 780.24$  nm,  $\Delta\lambda_{Lat} = 0.9$  nm,  $\eta = 5.0$ ,  $N_0 = 7.0 \times 10^{11}$  cm $^{-3}$ , and  $d_{23} = 1.0357 \times 10^{-29}$  Cm.

tively. The Rabi frequencies (detunings) for the probe and coupling fields are denoted by  $\Omega_p = \mathbf{E}_p \cdot \mathbf{d}_{13}/2\hbar$  ( $\Delta_p = \omega_{31} - \omega_p$ ) and  $\Omega_c = \mathbf{E}_c \cdot \mathbf{d}_{23}/2\hbar$  ( $\Delta_c = \omega_{32} - \omega_c$ ), where  $\mathbf{d}_{ij}$  and  $\omega_{ij}$  are the dipole moments and resonant frequencies for the relevant transitions, respectively. The levels  $|1\rangle$ ,  $|2\rangle$ , and  $|3\rangle$ , respectively, could correspond to  $|5S_{1/2}, F=1, m_F=1\rangle$ ,  $|5S_{1/2}, F=2, m_F=2\rangle$ , and  $|5P_{3/2}, F=2, m_F=2\rangle$  in D2 line of  $^{87}\text{Rb}$  atoms. Thus, the probe field is  $\sigma^+$  polarized, while the coupling field is  $\pi$  polarized.

Within the rotating wave and electric dipole approximations, the interaction Hamiltonian of the system can be expressed as

$$H_I = \hbar[(\Delta_p - \Delta_c)|2\rangle\langle 2| + \Delta_p|3\rangle\langle 3|] - \hbar[\Omega_p|3\rangle\langle 1| + \Omega_c|3\rangle\langle 2| + h.c.]. \quad (1)$$

The steady-state probe susceptibility  $\chi(x)$  of each filled cell can be obtained by solving the density matrix equation of  $\Lambda$ -type atoms, given by

$$\chi(x) = \frac{N(x)\mathbf{d}_{13}^2}{\hbar\epsilon_0} \frac{1}{\zeta}, \quad (2)$$

where  $\zeta = \frac{|\Omega_c|^2}{\Delta_p - \Delta_c - i\gamma_{21}} - i\gamma_{31}$ . Here,  $\gamma_{ij} = (\Gamma_i + \Gamma_j)/2$  are the coherence dephasing rates with the relevant population decay rates  $\Gamma_i$  and  $\Gamma_j$ . The spatial atomic density  $N(x)$ , which can be considered as a Gaussian distribution

in each filled cell, is given by

$$N(x) = \frac{N_0\lambda_0}{\sigma_x\sqrt{2\pi}} \cdot e^{[-(x-x_0)^2/2\sigma_x^2]}, \quad (3)$$

where  $N_0$  is the average atomic density,  $x_0$  is the trap center,  $\sigma_x = \lambda_{Lat}/(2\pi\sqrt{\eta})$  is the half-width with  $\eta = 2U_0/(\kappa_B T)$  related to the capture depth  $U_0$  and temperature  $T$ .  $\lambda_0 = \lambda_{Lat}/2$  is the width of each cell, with  $\lambda_{Lat}$  being the wavelength of a red-detuned retroreflected laser beam forming the optical lattice. For the Bragg condition, the incident angle is given by  $\theta = \arccos(\lambda_p/\lambda_{Lat0})$ , where  $\lambda_{Lat0} = \lambda_{Lat} - \Delta\lambda_{Lat}$  with the geometric Bragg shift  $\Delta\lambda_{Lat}$ . It is worth emphasizing that the condition for trapping atoms is  $\lambda_{Lat} > \lambda_{31}$  with  $\lambda_{31}$  being the wavelength of the transition  $|3\rangle \leftrightarrow |1\rangle$ .

The reflection and transmission properties of the defective lattice can be effectively characterized by a  $2 \times 2$  unimodular transfer matrix [41]. For filled lattice cells, we divide each cell into sufficient thin layers so that each layer can be regarded as homogeneous [42, 43]. The transfer matrix  $m(x_j)$  of a single layer can be expressed with the transmission and reflection coefficient as  $t(x_j) = 1/m(2,2)$ ,  $r_l(x_j) = m(1,2)/m(2,2)$  [ $r_r(x_j) = m(2,1)/m(2,2)$ ] on the left (right) side of this layer. These coefficients are dependent on the Fresnel coefficients, layer thickness, and the layer's reflective index  $n_f(x) = \sqrt{1 + \chi(x)}$  [44, 45]. For the homogeneous and thin layer,  $r_l(x_j) = r_r(x_j) \equiv r(x_j)$ . Thus,  $m(x_j)$  can be written as

$$m(x_j) = \frac{1}{t(x_j)} \begin{bmatrix} (t(x_j)^2 - r(x_j)^2) & r(x_j) \\ -r(x_j) & 1 \end{bmatrix}. \quad (4)$$

Here,  $t(x_j)$  and  $r(x_j)$  are the transmission and reflection coefficients of  $j$ th layer in each lattice cell with  $j \in [1, 100]$ . The transfer matrix of one filled cell can be expressed as

$$M_f = \prod_{j=1}^{100} m(x_j). \quad (5)$$

The refractive index  $n_v \equiv 1$  for vacant lattice cells. Thus, the transfer matrix of a vacant cell can be written as

$$M_v = \frac{1}{t(x)} \begin{bmatrix} t(x)^2 & 0 \\ 0 & 1 \end{bmatrix} = \begin{bmatrix} e^{ik\lambda_0} & 0 \\ 0 & e^{-ik\lambda_0} \end{bmatrix}. \quad (6)$$

Then, the total transfer matrix is expressed as

$$M_d = [(M_f)^{a_f} * (M_v)^{a_v}]^{p_1} * (M_f)^{p_2}. \quad (7)$$

For a perfect atomic lattice with the same length  $L$ , where each cell traps atoms with an identical distribution as Eq. 3, the total matrix can be written as

$$M_p = \prod_{k=1}^S M_f. \quad (8)$$

It is evident that this lattice exhibits the same reflectivities on both sides [38].

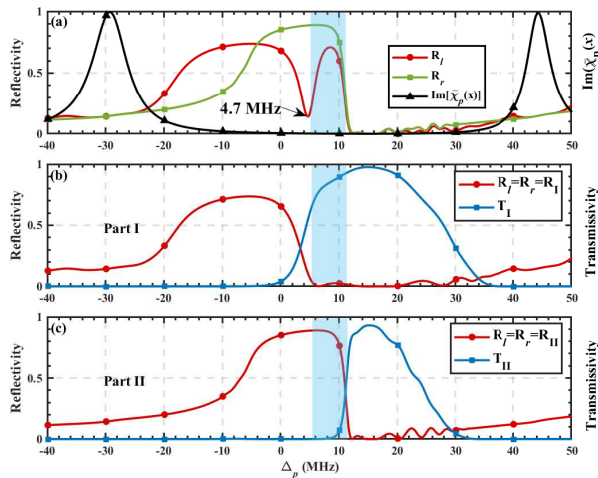


FIG. 2. (Color online) (a) Reflectivities  $R_{l,r}$  and imaginary part of average probe susceptibility  $\overline{\chi(x)}$  versus probe detuning  $\Delta_p$  in the defective atomic lattice. (b) Reflectivity  $R_I$  and transmissivity  $T_I$  for an individual lattice of Part I; (c) Reflectivity  $R_{II}$  and transmissivity  $T_{II}$  for an individual lattice of Part II versus detuning  $\Delta_p$ . Here  $a_f = 50$ ,  $a_v = 100$ ,  $p_1 = 10$  and  $p_2 = 1500$ , and other parameters are the same as Fig. 1.

In further, we can calculate the reflection coefficient  $r_l$  ( $r_r$ ) and transmission coefficient  $t$  on the left (right) of the lattice, which are given by

$$r_l = \frac{M_i(1,2)}{M_i(2,2)}, r_r = \frac{M_i(2,1)}{M_i(2,2)}, t = \frac{1}{M_i(2,2)}, \quad (9)$$

where  $i = p, d$ . Then, the relevant transmissivity  $T = |t|^2$ , reflectivities  $R_{l,r} = |r_{l,r}|^2$  and absorptivities  $A_{l,r} = 1 - T - R_{l,r}$ .

Using Eqs. (7) and (8), we can predict and compare the reciprocity of the probe reflection between the defective and perfect lattices, with  $|M_{d,p}(1,2)|^2$  and  $|M_{d,p}(2,1)|^2$  as functions of length  $L$  as shown in Fig. 1(c). While  $|M_p(1,2)| \equiv |M_p(2,1)|$ ,  $|M_{d,p}(1,2)|$  and  $|M_{d,p}(2,1)|$  gradually separate as  $L$  increases. This implies that the reflection reciprocity on both sides could be broken by eliminating atoms in some cells to induce the breaking of spatial symmetry for the lattice, which can be observed by assessing the reflectivities  $R_{l,r}$ .

Fig. 2(a) illustrates the deviation of the left-side (LS) and right-side (RS) reflectivities  $R_{l,r}$ , resulting in the reflection nonreciprocity in the defective atomic lattice with the lengths of Part I and Part II are equal to 0.585 mm and then  $L = 1.17$  mm. The high reflectivities of both sides are located within the EIT window  $\Delta_p \in (-20 \text{ MHz}, 40 \text{ MHz})$ , where atomic absorption is suppressed, indicated by the imaginary part of the average susceptibility  $\overline{\chi(x)}$  near zero. At  $\Delta_p = 4.70$  MHz, the reflectivity deviation reaches a maximum corresponding to  $R_l = 13.90\%$  and  $R_r = 88.66\%$ . While the RS reflection band is continuous, the LS reflection is divided by the valley into a wide platform and a narrow peak in the

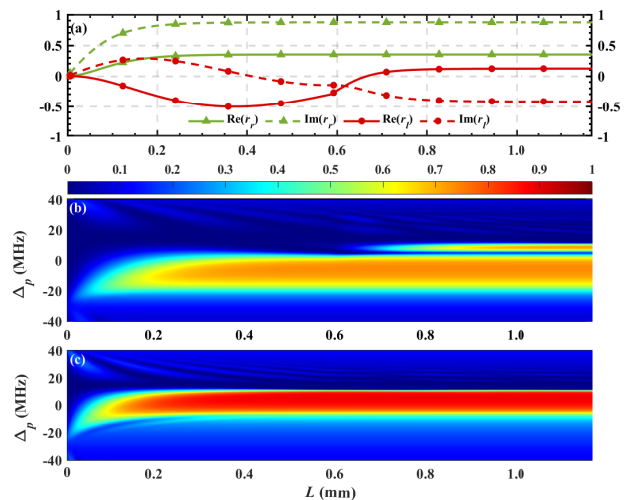


FIG. 3. (Color online) (a) Reflection coefficients  $r_{l,r}$  versus length  $L$  with  $\Delta_p = 4.7$  MHz. (b) Reflectivity  $R_l$  and (c) reflectivity  $R_r$  as functions of probe detuning  $\Delta_p$  and length  $L$ . The parameters are the same as Fig. 2.

shaded region.

In order to investigate the origin of nonreciprocal PBGs, we present the reflectivities and transmissivities for Part I (II) considered as an individual lattice with a length of 0.585 mm in Figs. 2(b) [2(c)]. The Bragg condition for the Part I lattice is given by

$$\frac{\omega_p}{c} (a_f \lambda_0 \overline{n_f(x)} + a_v \lambda_0 n_v) = k\pi, \quad (10)$$

with the vacuum speed of light  $c$ , an arbitrary positive integer  $k$ , and average refractive index  $\overline{n_f(x)}$  for a filled cell. Since  $\overline{n_f(x)} > n_v = 1$ , it follows that  $(a_f + a_v) \lambda_0 \overline{n_f(x)} > a_f \lambda_0 \overline{n_f(x)} + a_v \lambda_0 n_v$ . This implies that the optical path will decrease when some filled cells are replaced by vacant cells, and then the frequency  $\omega_p$  should increase, that is,  $\Delta_p$  decrease, to satisfy the Bragg condition again. Therefore, compared to the reflection  $R_{II}$  of the lattice of Part II [see Fig. 2(c)], the reflection band  $R_I$  of the lattice of Part I is blue-shifted [see Fig. 2(b)]. We note the reflection bands of  $R_r$  in Fig. 2(a) and  $R_{II}$  in Fig. 2(c) coincide because the right-incident light propagating along the defective lattice firstly encounters Part II and is then perfectly reflected. Additionally,  $R_l$  in Fig. 2(a) and  $R_I$  in Fig. 2(b) do except the narrow peak of  $R_l$  in the shaded regions. The underlying physics of forming the narrow band is that Part I is transparent for the left-incident light carrying frequencies in the shaded region [see  $T_I$  in Fig. 2(b)], and therefore, the light could pass Part I and be reflected backwards to the left side by Part II [see  $R_{II}$  in Fig. 2(c)].

We focused on reflection behaviors at the valley point  $\Delta_p = 4.7$  MHz. Fig. 3(a) illustrates that the real and imaginary parts of the reflection coefficient  $r_r$  for the right-incident light monotonically increase as the lattice length increases, which can be used to check the reflec-

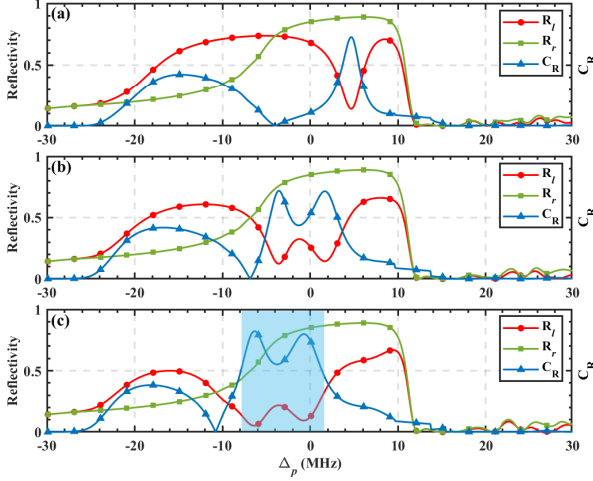


FIG. 4. (Color online) Reflectivities  $R_{l,r}$  and the reflection contrast  $C_R$  versus probe detuning  $\Delta_p$  with (a)  $a_v/a_f = 2$ , (b)  $a_v/a_f = 4$ , and (c)  $a_v/a_f = 6$ . Here  $a_f = 50$ ,  $p_1 = 10$  and  $p_2 = 1500$ , other parameters are the same as in Fig. 1.

tion on the end of the medium. After  $L \approx 0.25$  mm, they exhibit an identical tendency towards their respective steady values. However, a noticeable non-monotonic variation is observed in the real and imaginary parts of  $r_l$  for the left-incident light. Due to the more complex periodic structure of Part I, they tend towards stability only after the light has entered Part II. As a result, a more extended lattice (approximately 0.75 mm) is required to attain their steady values. Such a nonreciprocity of two-side reflections is caused by the lack of conjugacy between complex transfer matrix elements  $M_d(1,2)$  and  $M_d(2,1)$ . The underlying physics is that the insertion of vacant cells on one side breaks the spatial symmetry of the lattice structure. The differences in the value, width, and position between the two reflection-band spectra of  $R_l$  and  $R_r$  with varying lengths are intuitively shown in Figs. 3(b) and (c). Note, as shown in Fig. 3(b), the narrow peak of  $R_l$  becomes visible and progressively stronger only after  $L = 0.6$  mm, indicating the extension of the lattice into Part II. This also demonstrates that the narrow peak of  $R_l$  arises from the cooperation between Part I and Part II.

As mentioned above, the deviation of the two-side reflection bands is evident at the valley point, which can be quantified by the reflection contrast, given by

$$C_R = \left| \frac{R_l - R_r}{R_l + R_r} \right|. \quad (11)$$

According to the Bragg condition for the whole defective lattice

$$\frac{\omega_p}{c} \left[ p_1(a_f \lambda_0 \overline{n_f(x)} + a_v \lambda_0 n_v) + p_2 \lambda_0 \overline{n_f(x)} \right] = k\pi, \quad (12)$$

To achieve high-quality nonreciprocal reflection or even unidirectional reflection, we can design and optimize the

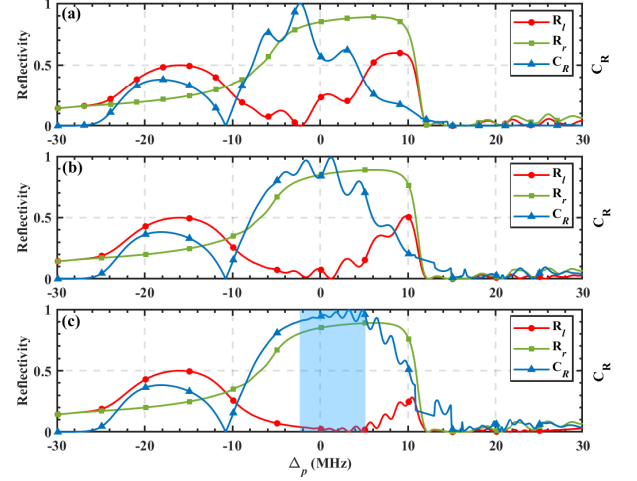


FIG. 5. (Color online) reflectivities  $R_{l,r}$  and the reflection contrast  $C_R$  versus probe detuning  $\Delta_p$  with (a)  $p_1 = 15$ , (b)  $p_1 = 30$ , and (c)  $p_1 = 70$ . Here  $a_f = 50$ ,  $a_v = 100$ , and  $p_2 = 1500$ , other parameters are the same as in Fig. 1.

structure of the defective lattice by adjusting  $a_{f,v}$  and  $p_{1,2}$ . Since vacant cells play a critical role, we change parameters relative to them, for example.

Increasing the ratio  $a_v/a_f$  in each period in Part I, accompanied by a decrease in the refractive index, can lead to a further blue shift for the wide platform in the LS reflection band. As shown in Fig. 4, the valley of the LS reflection band gradually blue-shifts with an increase of  $a_v/a_f$ . Consequently, the narrow peak in the LS reflection band, mainly due to Part II, widens but does not weaken significantly with the changes in Part I. However, the wide platform blue-shifts and weakens, gradually leaving the EIT regime. As  $a_v/a_f$  increases from 2 to 6, the band of high reflection contrast  $C_R$  gradually blue-shifts, widens to a certain extent and ultimately produces a broad band of  $C_R$  over 50% as shown in the shade region in Fig. 4(c). This allows for broadband nonreciprocal devices. Especially, with  $a_v/a_f = 6$ ,  $C_R$  can reach the maximum 83.50% at  $\Delta_p = -6.30$  MHz. This indicates the realization of a perfect unidirectional photonic reflector based on PBGs. Meanwhile, the RS reflection band remains unchanged. This can be explained further by considering instances in which the right-incident field propagates through and is Bragg-scattered by Part II of 1500 continuous filled cells, which is sufficient to support a high PBG without any influence from part I; however, the reflection spectra of LS probe field is primarily altered by Part I and partially affected by Part II.

To further optimize the nonreciprocal reflection band of high  $C_R$ , one feasible approach is to suppress the LS reflection band overlapping the RS one. This can be achieved without compromising the nonreciprocity by adjusting the number  $p_1$  of periods of part I. Figure 5 demonstrates that increasing  $p_1$  can significantly enhance the perfect nonreciprocal reflection band, as indicated by



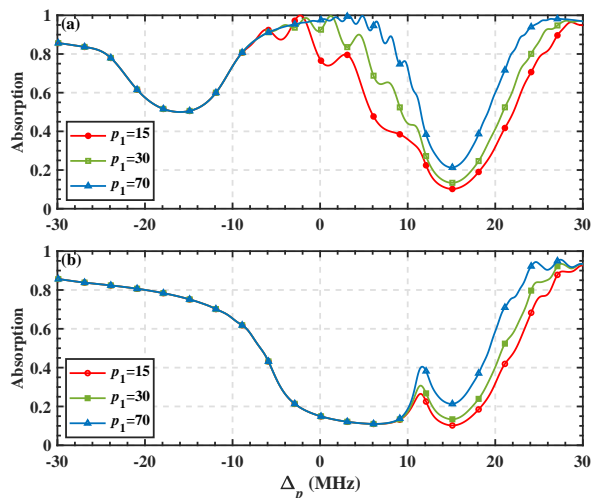


FIG. 6. (Color online) (a) Absorptivity  $A_l$  and (b) absorptivity  $A_r$  versus probe detuning  $\Delta_p$  with  $p_1 = 15$ ,  $p_1 = 30$ , and  $p_1 = 70$ . Here  $a_f = 50$ ,  $a_v = 100$ , and  $p_2 = 1500$ , other parameters are the same as in Fig. 1

high  $C_R$ . With  $p_1 = 70$ , the nonreciprocal reflection band of  $C_R \geq 90.0\%$  covers  $\Delta_p \in [-2 \text{ MHz}, 5 \text{ MHz}]$ , as shown in the shaded region in Fig. 5(c). It is noteworthy that this nonreciprocal band is also within the RS reflection band of high  $R_r$  while the LS reflection is effectively restrained.  $C_R \simeq 100\%$  can be achieved at certain points where  $R_l \simeq 0$ . Hence, such a unidirectional reflector scheme offers some advantages, such as broadband performance, and high reflectivity of unidirection.

Finally, to explain the strong suppression of LS reflection in the perfect nonreciprocal band, we plot the absorptivities  $A_l$  and  $A_r$  for left- and right-incident fields, respectively, in Figs. 6. As shown in 6(a), the absorption for the left-incident field in the perfect nonreciprocal band gradually increases with the period number  $p_1$  while the absorption for the right-incident field remains unchanged. This suggests that the increasing pe-

riod number  $p_1$  can induce one-way absorption enhancement that results in the complete one-way suppression of reflection. The main reason for this is that as  $p_1$  increase, more atoms can be introduced by the added filled cells, and the left-incident field of frequency in the narrow peak of  $R_l$  will experience much more absorption propagating forward and backward through Part I.

In summary, we propose a unidirectional photonic reflector scheme realized with a 1D defective atomic lattice of  $^{87}\text{Rb}$  atoms by intentionally designing some lattice cells to prevent atom trapping. The defective lattice consists of two parts of periodic structures. Part I, is a periodic structure where vacant cells appear periodically, while Part II, is a periodic structure where all cells are filled. The spatial symmetry is broken due to the distinct positions of the two parts. When considering two parts with the same cells, the vacant cells induce a blue shift of the reflection band of Part I relative to the reflection band of Part II. Consequently, the reflection nonreciprocity arises in such a defective lattice. Unlike the reflection band  $R_r$ , mainly arising from Part II and a wide platform in the band  $R_l$  mainly attributed to Part I, a narrow peak appears in band  $R_l$  due to the cooperation of Part I and II. The suppression of the narrow peak of  $R_l$ , by adjusting the ratio of numbers of vacant and filled cells in each period of Part I and the period number of Part I, allows us to obtain a broad nonreciprocal reflection band of high reflection contrast. Our feasible scheme arising from the breaking of spatial symmetry can be used to study some nonreciprocity problems. It also gives rise to potential avenues for realizing some all-optical nonreciprocal circuits and devices, such as optical diodes and isolators, one-way filters, and routers.

This work is supported by the Hainan Provincial Natural Science Foundation of China (Grant No. 121RC539) and the National Natural Science Foundation of China (Grant Nos. 12204137, 12126314, 12126351). This project is also supported by the specific research fund of The Innovation Platform for Academicians of Hainan Province Grant (No.YSPTZX202215).

[1] A. B. Khanikaev and A. Alù, Optical isolators: nonlinear dynamic reciprocity, *Nat. Photon.* **9**, 359 (2015).  
 [2] Y.-Q. Zhang, D. Zhang, Z. Zhang, C. Li, Y. Zhang, F. Li, M. R. Belić, and M. Xiao, Optical Bloch oscillation and Zener tunneling in an atomic system, *Optica* **4**, 571 (2017).  
 [3] H. Tian, J.-Q. Liu, A. Siddharth, R.-N. Wang, T. Blésin, J.-J. He, T. J. Kippenberg, and S. A. Bhave, Magnetic-free silicon nitride integrated optical isolator, *Nat. Photon.* **15**, 828 (2021).  
 [4] D. B. Sohn, O. E. Örsel, and G. Bahl, Electrically driven optical isolation through phonon-mediated photonic Autler-Townes splitting, *Nat. Photon.* **15**, 822 (2021).  
 [5] N. O. Antoniadis, N. Tamm, T. Jakubczyk, R. Schott, S.

R. Valentin, A. D. Wieck, A. Ludwig, R. J. Warburton, and A. Javadi, A chiral one-dimensional atom using a quantum dot in an open microcavity, *npj Quantum. Inf.* **8**, 27 (2022).  
 [6] L. Jin and Z. Song, Incident Direction Independent Wave Propagation and Unidirectional Lasing, *Phys. Rev. Lett.* **121**, 073901 (2018).  
 [7] G.-W. Lin, S.-C. Zhang, Y.-Q. Hu, Y.-P. Niu, J.-B. Gong, and S.-Q. Gong, Nonreciprocal Amplification with Four-Level Hot Atoms, *Phys. Rev. Lett.* **123**, 033902 (2019).  
 [8] J. Wu, Z.-M. Wang, H. Zhai, Z.-X. Shi, X.-H. Wu, and F. Wu, Near-complete violation of Kirchhoff's law of thermal radiation in ultrathin magnetic Weyl semimetal films, *Opt. Mater. Express* **11**, 4058 (2021).  
 [9] P. Lodahl, S. Mahmoodian, S. Stobbe, A. Rauschenbeutel, P. Schneeweiss, J. Volz, H. Pichler, and P. Zoller, Chi-

- ral quantum optics, *Nature (London)* **541**, 473 (2017).
- [10] M. Litinskaya and E.-A. Shapiro, Negative refraction and photonic-crystal optics in a cold gas, *Phys. Rev. A* **91**, 033802 (2015).
- [11] Y.-T. Chen, L. Du, L. Guo, Z. Wang, Y. Zhang, Y. Li, and J.-H. Wu, Nonreciprocal and chiral single-photon scattering for giant atoms, *Commun. Phys.* **5**, 215 (2022).
- [12] P.-F. Yang, X.-W. Xia, H. He, S.-K. Li, X. Han, P. Zhang, G. Li, P.-F. Zhang, J.-P. Xu, Y.-P. Yang, and T.-C. Zhang, Realization of Nonlinear Optical Nonreciprocity on a Few-Photon Level Based on Atoms Strongly Coupled to an Asymmetric Cavity, *Phys. Rev. Lett.* **123**, 233604 (2019).
- [13] E. Verhagen and A. Alù, Optomechanical nonreciprocity, *Nat. Phys.* **13**, 922 (2017).
- [14] C. Jiang, L.-N. Song, and Y. Li, Directional amplifier in an optomechanical system with optical gain, *Phys. Rev. A* **97**, 053812 (2018).
- [15] Y.-T. Chen, L. Du, Y.-M. Liu, Y. Zhang, Dual-gate transistor amplifier in a multimode optomechanical system, *Optics Express* **28**, 7095 (2020).
- [16] H. Yang, G.-Q. Qin, H. Zhang, X. Mao, M. Wang, and G.-L. Long, Multimode interference induced optical nonreciprocity and routing in an optical microcavity, *Ann. Phys.* **533**(5), 2000506, (2021).
- [17] C. Kong, H. Xiong, and Y. Wu, Magnon-Induced Nonreciprocity Based on the Magnon Kerr Effect, *Phys. Rev. Applied* **12**, 034001 (2019).
- [18] C. Kong, J. Liu, and H. Xiong, Nonreciprocal microwave transmission under the joint mechanism of phase modulation and magnon Kerr nonlinearity effect, *Front. Phys.* **18**, 12501 (2023).
- [19] L. Tang, J.-S. Tang, M.-Y. Chen, F. Nori, M. Xiao, and K.-Y. Xia, Quantum squeezing induced optical nonreciprocity, *Phys. Rev. Lett.* **128**, 083604 (2022).
- [20] S.-C. Zhang, Y.-Q. Hu, G.-W. Lin, Y.-P. Niu, K.-Y. Xia, J.-B. Gong, and S.-Q. Gong, Thermal-motion-induced non-reciprocal quantum optical system, *Nat. Photonics* **12**, 744 (2018).
- [21] G.-W. Lin, S.-C. Zhang, Y.-Q. Hu, Y.-P. Niu, J.-B. Gong, and S.-Q. Gong, Nonreciprocal Amplification with Four-Level Hot Atoms, *Phys. Rev. Lett.* **123**, 033902 (2019).
- [22] Y.Q. Hu, Y.-H. Qi, L. You, S.-C. Zhang, G.-W. Lin, X.-L. Li, J.-B. Gong, S.-Q. Gong, and Y.-P. Niu, Passive nonlinear optical isolators by passing dynamic reciprocity, *Phys. Rev. A* **16**, 014046 (2021).
- [23] L. Yang, Y. Zhang, X.-B. Yan, Y. Sheng, C.-L. Cui, and J.-H. Wu, Dynamically induced two-color nonreciprocity in a tripod system of a moving atomic lattice, *Phys. Rev. A* **92**, 053859 (2015).
- [24] S. A. R. Horsley, J.-H. Wu, M. Artoni, and G. C. La Rocca, Optical Nonreciprocity of Cold Atom Bragg Mirrors in Motion, *Phys. Rev. Lett.* **110**, 223602 (2013).
- [25] D.-W. Wang, H.-T. Zhou, M.-J. Guo, J.-X. Zhang, J. Evers, and S.-Y. Zhu, Optical Diode Made from a Moving Photonic Crystal, *Phys. Rev. Lett.* **110**, 093901 (2013).
- [26] Y.-M. Liu, F. Gao, C.-H. Fan, and J.-H. Wu, Asymmetric light diffraction of an atomic grating with PT symmetry, *Opt. Lett.* **42**, 4283 (2017).
- [27] J.-H. Wu, M. Artoni, and G. C. La Rocca, Parity-time-antisymmetric atomic lattices without gain, *Phys. Rev. A* **91**, 033811 (2015).
- [28] J.-H. Wu, M. Artoni, and G. C. La Rocca, Non-Hermitian Degeneracies and Unidirectional Reflectionless Atomic Lattices, *Phys. Rev. Lett.* **113**, 123004 (2014).
- [29] Y. Zhang, J.-H. Wu, M. Artoni, and G.-C. La Rocca, Controlled unidirectional reflection in cold atoms via the spatial Kramers-Kronig relation, *Opt. Express* **29**(4), 5890-5900 (2021).
- [30] S. A. R. Horsley, M. Artoni, and G. C. La Rocca, Spatial Kramers-Kronig relations and the reflection of waves, *Nat. Photon.* **9**(7), 436-439 (2015).
- [31] S. Longhi, Bidirectional in visibility in Kramers-Kronig optical media, *Opt. Lett.* **41**(16), 3727-3730 (2016).
- [32] R. Taubert, D. Dregely, T. Stroucken, A. Christ, and H. Giessen, Octave-wide photonic band gap in three-dimensional plasmonic Bragg structures and limitations of radiative coupling, *Nat. Commun.* **3**, 691 (2012).
- [33] J. Zhu, C. Bian, Z. Zhao, X.-D. Zhao, L. Qin, Y.-Y. Zhang, L. Zhou, and G. Dong, Saturation of superradiant light scattering from an atomic grating with a large number of atoms, *Phys. Rev. A* **106**, 013312 (2022).
- [34] A. Schilke, C. Zimmermann, P. W. Courteille and W. Guerin, Photonic Band Gaps in One-Dimensionally Ordered Cold Atomic Vapors, *Phys. Rev. Lett.* **106**, 223903 (2011).
- [35] N. V. Corzo, B. Gouraud, A. Chandra, A. Goban, A. S. Sheremet, D. V. Kupriyanov, and J. Laurat, Large Bragg Reflection from One-Dimensional Chains of Trapped Atoms Near a Nanoscale Waveguide, *Phys. Rev. Lett.* **117**, 133603 (2016).
- [36] G. Natale, T. Bland, S. Gschwendtner, L. Lafforgue, D. S. Grün, A. Patscheider, M. J. Mark, and F. Ferlaino, Bloch oscillations and matter-wave localization of a dipolar quantum gas in a one-dimensional lattice, *Commun. Phys.* **5**, 227 (2022).
- [37] A. Schilke, C. Zimmermann, and W. Guerin, Photonic properties of one-dimensionally-ordered cold atomic vapors under conditions of electromagnetically induced transparency, *Phys. Rev. A* **86**, 023809 (2012).
- [38] H. Yang, L. Yang, X.-C. Wang, C.-L. Cui, Y. Zhang, and J.-H. Wu, Dynamically controlled two-color photonic band gaps via balanced four-wave mixing in one-dimensional cold atomic lattices, *Phys. Rev. A* **88**, 063832 (2013).
- [39] H. Yang, T.-G. Zhang, Y. Zhang, and J.-H. Wu, Dynamically tunable three-color reflections immune to disorder in optical lattices with trapped cold  $^{87}\text{Rb}$  atoms, *Phys. Rev. A* **101**, 053856 (2020).
- [40] T.-M. Li, M.-H. Wang, C.-P. Yin, J.-H. Wu, and H. Yang, Dynamic manipulation of three-color light reflection in a defective atomic lattice, *Opt. Express* **29** 31767 (2021).
- [41] M. Artoni, G. C. La Rocca, and F. Bassani, Resonantly absorbing one-dimensional photonic crystals, *Phys. Rev. E* **72**, 046604 (2005).
- [42] M. Artoni and G. C. La Rocca, Optically Tunable Photonic Stop Bands in Homogeneous Absorbing Media, *Phys. Rev. Lett.* **96**, 073905 (2006).
- [43] Y. Zhang, Y. Xue, G. Wang, C.-L. Cui, R. Wang, J.-H. Wu, Steady optical spectra and light propagation dynamics in cold atomic samples with homogeneous or inhomogeneous densities, *Opt. Express* **19**, 2111-2119 (2011).
- [44] M. Born and E. Wolf, *Principles of Optics*, 6th ed. Cambridge University Press, Cambridge, UK, (1980).
- [45] A. S. Kuraptsev, and I. M. Sokolov, Reflection of resonant light from a plane surface of an ensemble of motionless point scatters: quantum microscopic approach, *Phys. Rev. A* **91**, 053822 (2015).